UNIVERSITÄT LEIPZIG

Leipzig Institute for Meteorology

Airborne hyperspectral observations using a commercial digital camera

A. Ehrlich[1], M. Wendisch[1], E. Bierwirth[1], J.-F. Gayet[2] and A. Herber[3]

[1] Leipzig Institute for Meteorology (LIM), University Leipzig, Germany
[2] Laboratoire de Météorologie Physique (LAMP), Université Blaise Pascal, Aubière Cedex, France
[3] Alfred Wegener Institute for Polar and Marine Research (AWI), Potsdam, Germany

a.ehrlich@uni-leipzig.de

Funded by DFG WE1900/17-1 and AWI

1. Introduction

Airborne Remote Sensing of Arctic Clouds and Sea Ice

- high impact of clouds and sea ice on Arctic energy budget
- high contrast between sea ice and open water
- interaction of clouds and sea ice in radiative transfer
  - discrimination of low clouds and sea ice is difficult
  - high uncertainties of cloud properties retrieved above ice

➔ **directional reflectivity may help to improve retrievals**

Fig. 1 Left: Photograph of glory and cloud bow. Right: MODIS image of sea ice and clouds.

SORPIC (Study on Solar Radiation and Phase Discrimination of Arctic Clouds)

- airborne remote sensing and in situ measurements with Polar 5 (AWI) in May 2010[1]
- operations from Spitsbergen with measurement area above Greenland sea
- remote sensing: SMART-Albedometer, AISA-Eagle, Canon camera, AMALi, AMSSP[1]
- in situ: Polar Nephelometer, CPI, FSSP-100, Nevzorov Probe[1]
- others: EM-Bird, sun photometer[1]

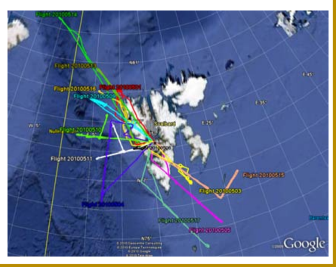

Fig. 2: SORPIC 2010 flight tracks.

2. CANON EOS-1D Mark III

Camera Specifications

- digital single-lens reflex camera
- CMOS sensor with 28.1×18.7mm sensor area
- 3908×2600 pixel
- wide-angle lens Canon EF 14mm f/2.8L II USM
- angle of view of Θ= 100.6°
- angular resolution of each pixel is about 0.025°

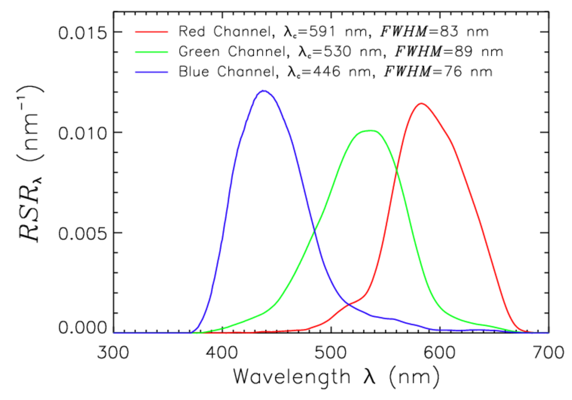

Fig. 2: Photograph and spectral characteristic in terms of the relative spectral response RSF$_\lambda$ of the canon camera [1].

Camera Settings

- raw data with 16 bit dynamic range
- exposure time 1/2656 s
- f-number of F/9.1,
- film speed of ISO-400

Post Processing

- radiometric calibration
- spectral calibration
- geometric correction of aircraft roll and pitch angle

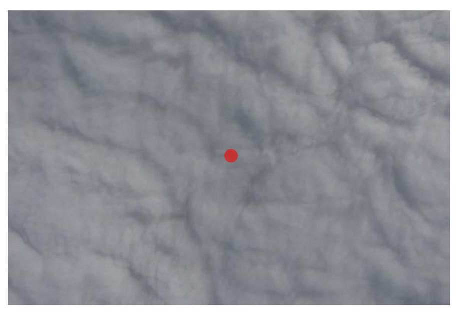

Fig. 3: Image taken by the camera. The red area indicates the spot of the radiance measurement covered by the SMART-Albedometer.

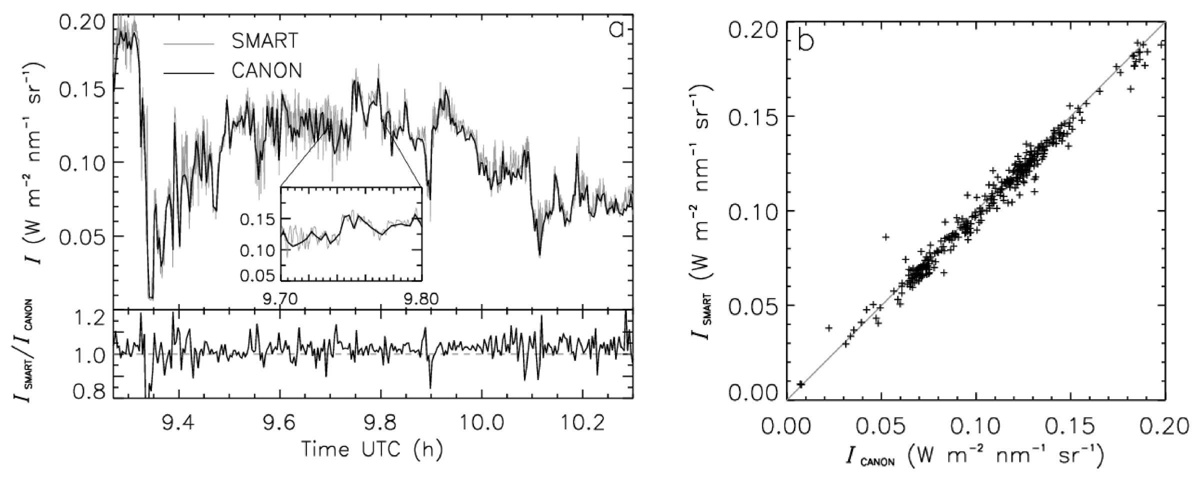

Figure 4: Comparison of nadir radiance measured by the camera and the SMART-Albedometer. The footprint of SMART-Albedometer is about 2.1 which corresponds to about 16 000 pixel of an image (see Fig. 3). These pixel were averaged for the comparison [1].

3. Hemispherical-Directional Reflectance Factor HDRF

- HDRF calculated with reflected radiance I_R from the camera and F_{glob} from the SMART-Albedometer

$$\mathrm{HDRF}(\theta_0,\varphi_0;2\pi;\theta_r,\varphi_r) = \pi\,\mathrm{sr}\cdot\frac{\mathrm{d}I_r(\theta_0,\varphi_0;2\pi;\theta_r,\varphi_r)}{\mathrm{d}F_{glob}(\theta_0,\varphi_0)}$$

- sequence of images were averaged
- depending on the heterogeneity of the surface less then 20 images are required

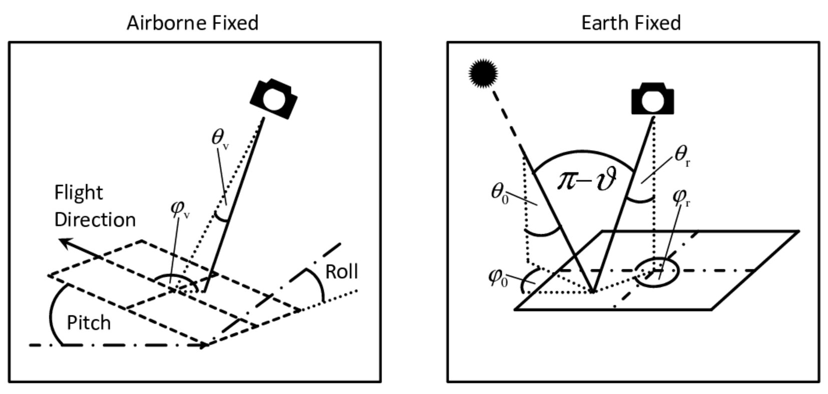

Figure 5: Geometry of the measurements [1].

Clouds

- 50 images of 17 May, 9:50 UTC
- 3100 m altitude
- θ_0= 56°, φ_0=166.5°

Sea Ice

- 46 images of 14 May, 8:25 UTC
- 100 m altitude
- θ_0= 67°, φ_0=123°

Open Water

- 11 images of 14 May, 10:22 UTC
- 3050 m altitude
- θ_0= 61°, φ_0=165.5°

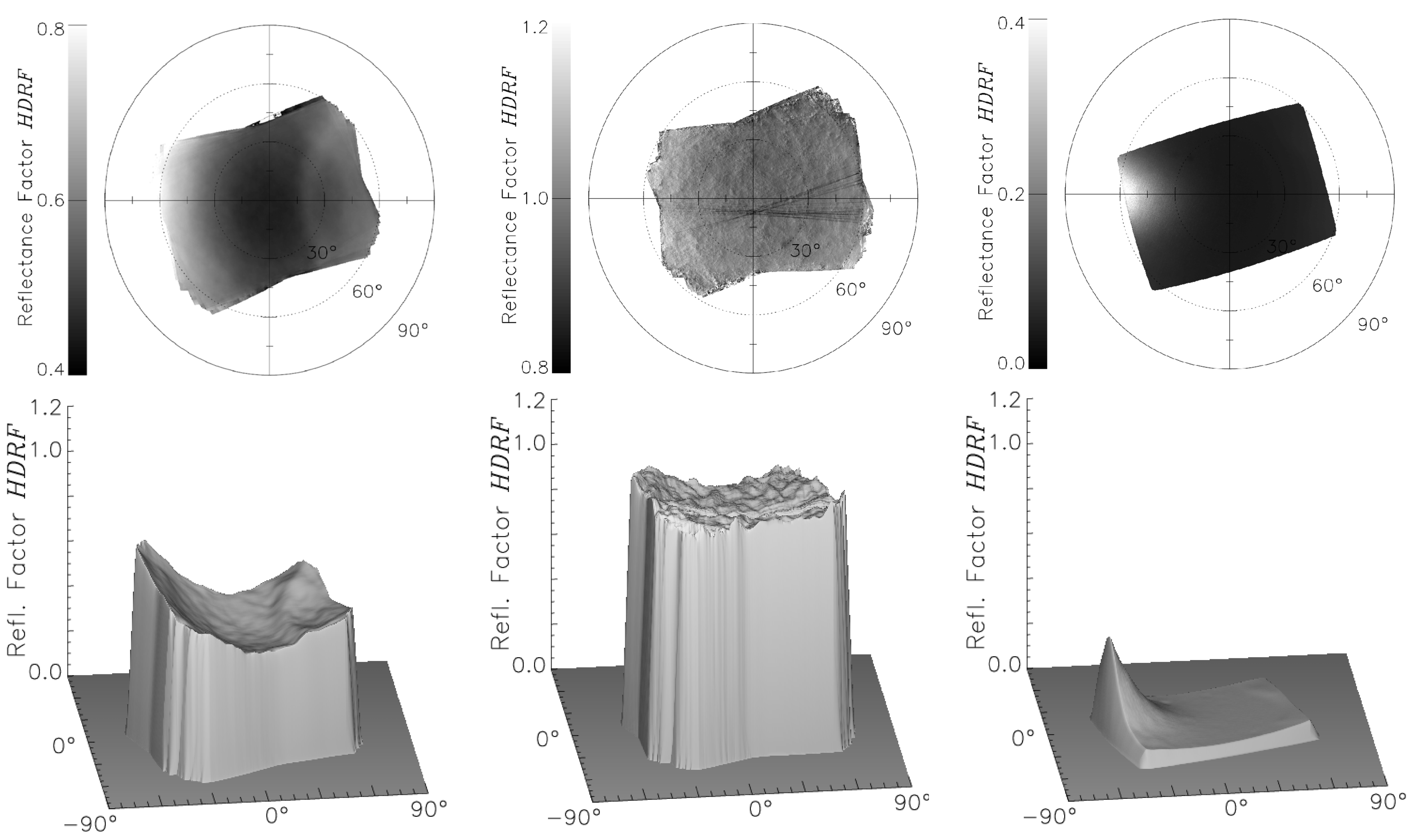

Figure 6: HDRF of clouds, sea ice and open water. The upper panels show polar plots while the 3D-plots in the lower panels indicate the shape of the HDRF [1].

4. Simulations for Open Water

Radiative Transfer Model

- plan parallel simulations (DISORT 2) using libRadtran
- BRDF parameterization based on Cox and Munk [2] and Nakajima and Tanaka [3]
- **variation of surface wind speed** between 5 ms^{-1} and 15 ms^{-1} (9 ms^{-1} was measured)

Results

- HDRF for flight altitude and surface (atmospheric correction)
- sun glint decreases with increasing surface wind speed
- ϑ > 80° agreement within measurement uncertainty
- ϑ < 80° **sun glint**, angular position matches simulations magnitude differs (calibration uncertainties)

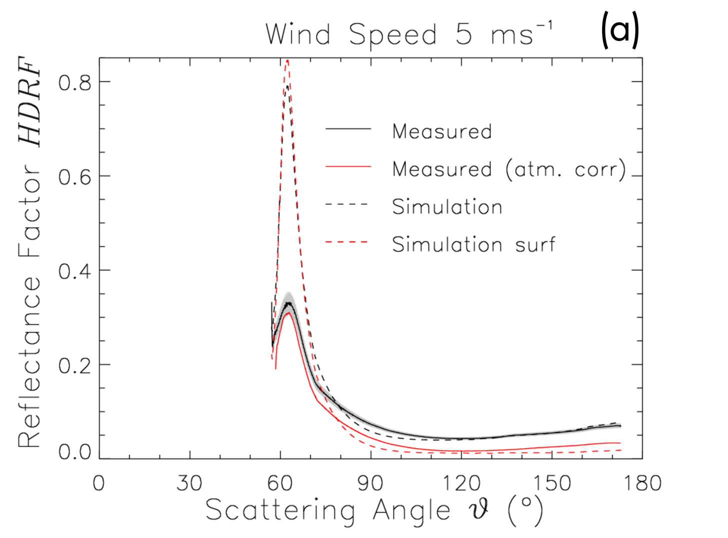

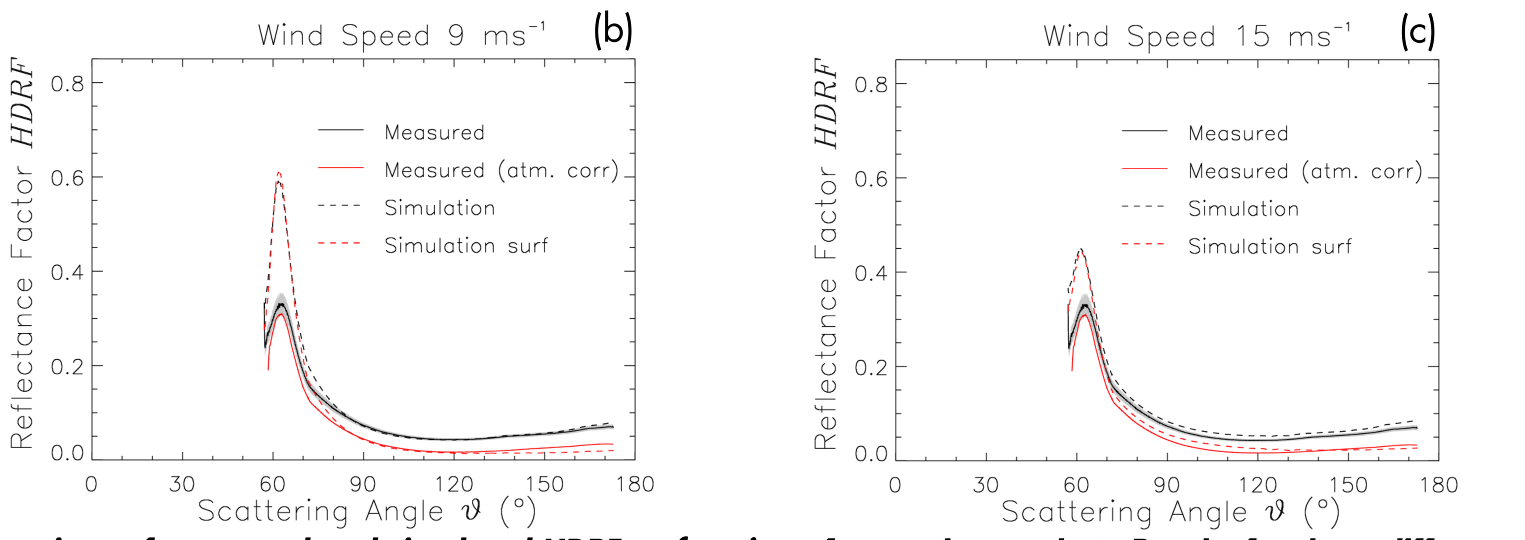

Fig. 7: Comparison of measured and simulated HDRF as function of scattering angle ϑ. Results for three different surface wind speeds are shown, (a) 5 ms^{-1}, (b) 9 ms^{-1}, (c) 15 ms^{-1}. HDFR at flight altitude is plotted black, surface HDRF is shown by red lines. The grey area indicates the measurement uncertainty [1].

5. Simulations for Clouds

Radiative transfer model:

- plan parallel simulations (DISORT 2) using libRadtran
- **variation cloud droplet effective radius R_{eff}** between 4 μm and 10 μm (R_{eff} = 9 μm measured by in situ instruments)

Results:

- **cloud bow** more pronounced for large cloud droplets in the simulations
- differences:
  → small and large scattering angles ➔ cloud inhomogeneities, 3d-effects
  → cloud bow: measurements indicate small cloud droplets

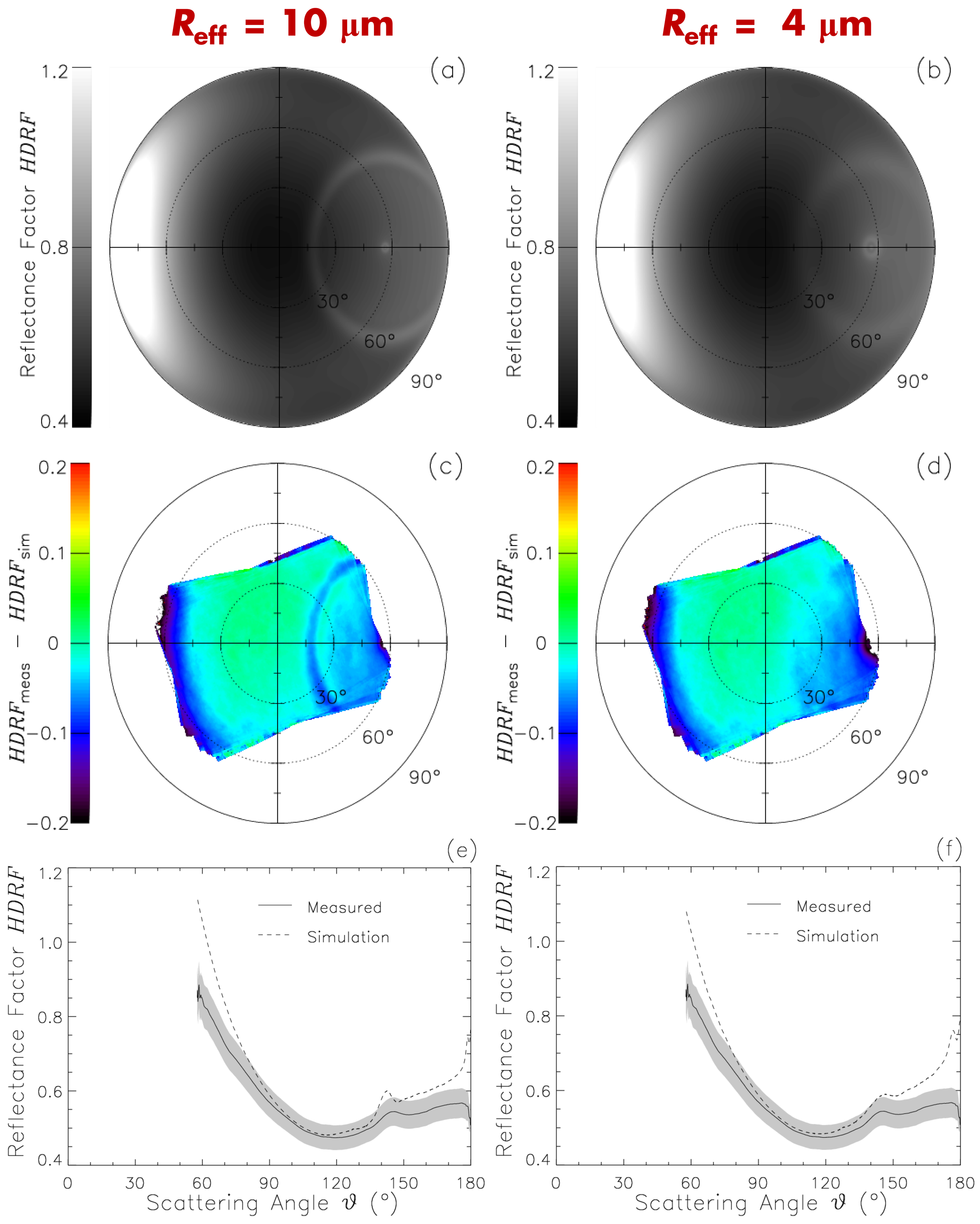

Fig. 8: Simulated and measured HDRF of clouds at 530 nm wavelength.

(a) and (b): Simulated HDRF are shown in panel (a) and (b) for R_{eff} = 10 μm (a) and R_{eff} = 4 μm (b).

(c) and (d): Color-coded differences between measured and simulated HDRF.

(e) and (f): Measured and simulated HDRF as function of scattering angle ϑ. The grey area indicates the measurement uncertainty [1].

6. Outlook

Improvements

- systematic retrieval of particle size
- circular flight patterns or **fish-eye lens** to extend field of view
- **polarization camera** for linear and circular polarization

VERDI (Study on the Vertical Distribution of Ice in Arctic Clouds)

- April/May 2012, Inuvik, Canada
- 13 flights above Beaufort sea (similar instrumentation to SORPIC)
- improved flight pattern, use of **AISA-Eagle** images

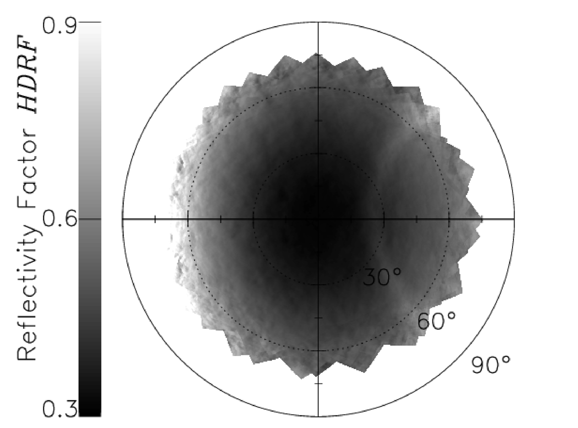

Fig. 9: HDRF of clouds derived from flying circles.

[1] Ehrlich, A., Bierwirth, E., Wendisch, M., Herber, A., and Gayet, J.-F. [2012]. Airborne hyperspectral observations of surface and cloud directional reflectivity using a commercial digital camera. Atmos. Chem. Phys., 12, 3493–3510.

[2] Cox, C. and Munk, W. [1954]. Measurement of the roughness of the sea surface from photographs of the sun's glitter, J. Opt. Soc. Am. A., 44, 838–850.

[3] Nakajima, T. and Tanaka, M. [1983]. Effect of wind-generated waves on the transfer of solar radiation in the atmosphere-ocean system, J. Quant. Spectrosc. Ra., 29, 521–537.